polymers

MDPI

Article

Synthesis of Novel Hyperbranched Polybenzo-Bisthiazole Amide with Donor–Acceptor (D-A) Architecture, High Fluorescent Quantum Yield and Large Stokes Shift

Xiaobing Hu

College of Chemistry and Chemical Engineering, Baoji University of Arts and Sciences, Shaanxi Province Key Laboratory of Phytochemistry, Baoji 721013, Shaanxi, China; hxb.0917@stu.xjtu.edu.cn; Tel.: +86-917-356-6589

Received: 23 June 2017; Accepted: 21 July 2017; Published: 25 July 2017

Abstract: Two novel highly fluorescent hyperbranched polybenzobisthiazole amides with a donor–acceptor architecture and large Stokes shift were rationally designed and synthesized. The chemical structures of the prepared hyperbranched polymers were characterized using Fourier Transform Infrared Spectroscopy (FTIR) analysis, Hydrogen Nuclear Magnetic Resonance (^{1}H-NMR) analysis, and Gel Permeation Chromatography (GPC) analysis. These two polymers were soluble in dimethyl sulfoxide (DMSO) and *N*,*N*-dimethylformamide (DMF), and their DMSO and DMF solutions emitted strong green light (517–537 nm) with high quantum yields (QYs) and large Stokes shifts. Their relative fluorescence QYs in the DMSO solution were calculated as 77.75% and 81.14% with the Stokes shifts of 137 nm (0.86 eV) and 149 nm (0.92 eV) for HP–COOH and HP–NH_2, respectively, using quinine sulfate as the standard. In the DMF solution, the QYs of HP–COOH and HP–NH_2 were calculated as 104.65% and 118.72%, with the Stokes shifts of 128 nm (0.79 eV) and 147 nm (0.87 eV), respectively. Their films mainly emitted strong blue light with the maximum emission wavelengths of 436 nm and 480 nm for HP–COOH and HP–NH_2, respectively. The Stokes shifts for HP–COOH and HP–NH_2 films were 131 nm (0.42 eV) and 179 nm (0.86 eV), respectively. They are promising candidates for luminescent solar concentrators and blue light emitting materials.

Keywords: hyperbranched polyamide; 1,3,5-tris(4-carboxyphenyl) benzene; fluorescence quantum yield; donor–acceptor architecture

1. Introduction

Over the past few decades, hyperbranched polymers have drawn continuous and considerable attention because of their unique molecular architecture, improved physical and chemical properties, and their broad range of applications, such as fluorescent probes [1–5], polymer coatings [6,7], Separation materials [8], drug or biomolecule carrier materials [9–16], and in optoelectronic materials and devices [17–26]. Compared to linear polymers, hyperbranched polymers have the obvious advantages of high solubility, little chain entanglement, low viscosity, good processability, tunable light emission, low crystallinity, and controllable thin film morphology [27,28]. They have highly branched architecture, and large numbers of functional terminal groups and nanoscale cavities, and they are superior to their dendritic counterparts because of their convenient "one-pot" synthesis and their potential for large-scale production [29]. Generally, two kinds of strategies are used to synthesize hyperbranched polymers: the AB_n (when $n \geq 2$) strategy and the $A_2 + B_n$ (when $n \geq 3$) strategy [30–32]. For the AB_n strategy, although gelation is easy to avoid in theory, the monomers are usually difficult to synthesize, because the molecules have two different reactive groups and they can undergo self-polymerization in some cases. The second strategy, $A_2 + B_n$, has certain merits,

specifically, this strategy uses commercially available monomers and results in high-yield soluble hyperbranched polymers synthesized by controlling the polymerization conditions and quenching the reaction before the gel point [33]. Therefore, the $A_2 + B_n$ route has become an important method for synthesizing hyperbranched polymers with wide applications.

Poly(*p*-phenylene benzobisthiazole) (PBZT) is a kind of aromatic heterocyclic conjugated polymer, which is well known for its excellent mechanical properties (high tensile strength and modulus), high chemical and thermo-oxidative stabilities [34], and large and ultrafast third-order nonlinear optics response [35–39]. PBZT is insoluble in common organic solvents because of the high degree of molecular rigidity and strong intermolecular interactions, making PBZT difficult to process and impeding further detailed and accurate studies on this type of conjugated polymer. Introducing hyperbranched structure into conjugated polymers is an effective strategy for solving this issue. In our previous work, hyperbranched structure was introduced into the PBZT backbone using the $A_2 + B_3$ method [39,40]. The prepared hyperbranched polybenzobisthiazoles were soluble in organic solvents, and their solutions emitted strong blue fluorescence [39,40].

In this contribution, two novel fluorescence hyperbranched polybenzobisthiazole amides with donor–acceptor (D-A) architecture were designed and synthesized using a direct polycondensation of 1,3,5-tris(4-carboxyphenyl) benzene (H_3BTB, acceptor) with 2,6-diaminobenzo[1,2-d:4,5-d′]bisthiazole (DABBT, donor) via the $A_2 + B_3$ approach. The non-planar globular topological structures of the designed polymers make their chromophoric repeat units difficult to pack in a compact and ordered fashion. Consequently, the π–π stacking interaction in the polymer aggregates will be effectively suppressed, which is beneficial for a higher light emitting efficiency [3,41]. Furthermore, the donor–acceptor (D-A) architecture along the conjugated polymer backbones will imparts intramolecular charge transfer character, the highest occupied molecular orbital (HOMO) and the lowest unoccupied molecular orbital (LUMO) optical transition and larger effective Stokes shifts, hence endow adjustable optoelectronic properties and high solid-state fluorescence [42–45]. The synthetic approach is shown in Scheme 1. The condensation polymerization of DABBT and H_3BTB was performed in two ways. Manner 1, DABBT and H_3BTB were added in a mole feed ratio of 1:1 (m:n = 1:1), in which the carboxyl-terminated hyperbranched polyamide (HP–COOH) was generated. When the mole feed ratio of DABBT and H_3BTB was 9:4 (Manner 2, m:n = 9:4), the amino-terminated hyperbranched polyamide (HP–NH_2) was prepared. These two hyperbranched polyamides exhibit high fluorescence emission quantum efficiency because of the aromatic heterocyclic benzobisthiazole groups or H_3BTB groups in their molecular structures which have displayed strong blue or green fluorescence in our previous studies, respectively [39,40,46]. These two polymers possess organo-solubility that allow for the facile and low-cost solution processing of an amorphous, highly luminescent thin film. Their relative QYs in DMSO and DMF solution were studied using quinine sulfate as the standard. The photophysical properties of the polymer thin films were also investigated.

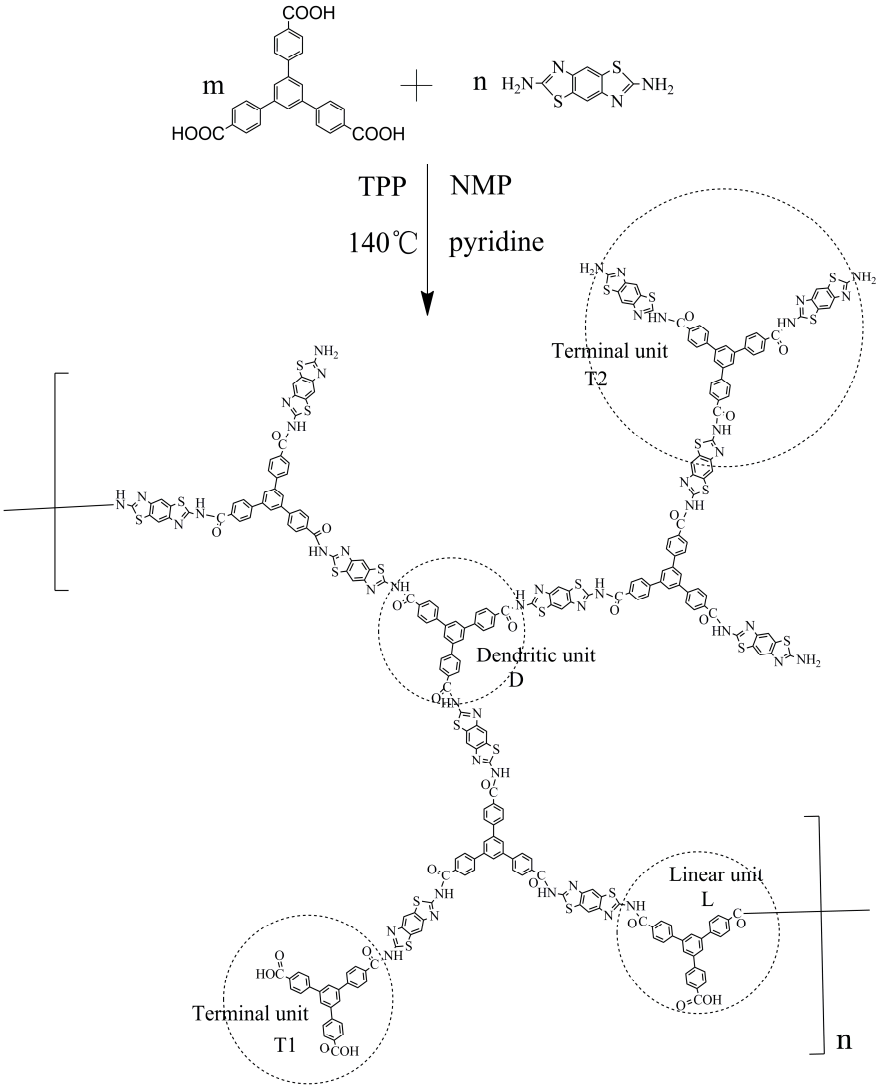

Scheme 1. Synthetic route of hyperbranched polybenzobisthiazole amide.

2. Materials and Methods

2.1. Starting Materials

DABBT was synthesized and purified using a slightly modified procedure reported in the literature [47,48]. The ^{1}H-NMR and ^{13}C-NMR spectra of DABBT are shown the Supplementary Materials (Figures S1 and S2). ^{1}H-NMR (400 MHz, DMSO-d_6, δ): 7.59 (s, 2H, Ar-H), 7.26 (s, 4H, –NH_2). ^{13}C-NMR (100 MHz, DMSO-d_6, δ): 110.02, 129.62, 148.12, 165.28. H_3BTB was synthesized using a two-step reaction as described in our previous work [40]. The ^{1}H-NMR and ^{13}C-NMR spectra of H_3BTB are shown in the Supplementary Materials (Figures S3 and S4). ^{1}H-NMR (400 MHz, DMSO-d_6, δ): 8.03 (m, 15H, Ar-H), 12.99 (s, 3H, –COOH); ^{13}C-NMR (100 MHz, DMSO-d_6, δ): 167.57, 144.25, 141.16, 130.47, 130.33, 127.83, 125.98. *N*-Methyl-pyrrolidone (NMP), triphenyl phosphite (TPP), and pyridine (Py) were purchased from Sinopharm Chemical Reagent Co., Ltd. (Shanghai, China) without further purification. Quinine sulfate was purchased from Adamas Reagent, Ltd (Shanghai, China) and used as received.

2.2. Polymerization

The condensation polymerization of DABBT and H_3BTB was performed in two manners with different mole feed ratios of the monomers as shown in Scheme 1. For the carboxyl-terminated

hyperbranched polyamide (HP–COOH), the mole feed ratio of DABBT and H_3BTB was 1:1, while for the amino-terminated hyperbranched polyamide (HP–NH_2), the mole feed ratio of DABBT and H_3BTB was 9:4. The specific reaction process was as follows. A 100 mL dry three-neck flask was purged with argon gas for 30 min. Then, 40 mL of N-methyl pyrrolidone (NMP), 3 mL of pyridine, 3.5 mL of triphenyl phosphite (TPP), and certain amounts of DABBT and H_3BTB were added to the flask with continuous stirring and dry argon purging. After the mixture was dissolved, the reaction mixture was heated step wise to 140 °C the polymerization was performed at this temperature for about 10 h. The reaction system was then cooled naturally to room temperature; absolute methanol was added, and stirred for another 30 min. The precipitate was collected by vacuum filtration and washed with deionized water several times. Finally, the polymer was extracted with deionized water in a Soxhlet apparatus for 24 h and then dried at 90 °C for 48 h under reduced pressure. The yields of HP–COOH and HP–NH_2 were 55.8% and 46.4%, respectively.

2.3. Measurements

^{1}H-NMR and ^{13}C-NMR spectra were recorded on a Varian 400 MHz NMR spectrometer using deuterated dimethyl sulfoxide (DMSO-d_6) as the solvent and tetramethylsilane (TMS) as an internal reference. Fourier transform infrared (FTIR) spectra were measured on a Perkin Amelmer infrared spectrometer at room temperature. GPC measurements were performed on a Waters 1515 GPC system under 35 °C, DMF was used as the eluent with a flow rate of 1.0 mL/min. The molecular weights and molecular weight distributions of the polymers were calculated using narrow-molecular-weight polystyrene standards as reference. UV–Vis absorption spectra of polymers in DMSO and DMF solutions were recorded on a Shimadzu UV-2550 spectrometer (Shimadzu Co., Ltd., Kyoto, Japan) over a wavelength range of 250–800 nm. Wide-angle powder X-ray diffraction (XRD) patterns were recorded at room temperature on a Rigaku Ultima IV X-ray (Rigaku Corporation, Tokyo, Japan) diffraction system using Cu Kα radiation (λ = 0.15406 nm), at a scanning rate of 2°/s. Thermogravimetric analyses (TGA) were recorded on a Perkin-Elmer (Perkin-Elmer Co., Ltd., Massachusetts, the United States) TG/DTA under nitrogen flow with a heating rate of 10 °C/min. The temperature range was from 30 to 800 °C. Differential scanning calorimetry (DSC) analyses were performed on a TA Instruments DSC Q200 (TA Instrument Co., Ltd., New Castle, the United States) using sealed aluminum sample pans and sealed aluminum reference pans at a heating rate of 10 °C/min under a nitrogen atmosphere. The temperature range was from −80 to 400 °C. Fluorescence spectra were recorded on a Horiba scientific Fluoromax-4 spectrofluorometer (HORIBA Scientific, Edison, the United States) using spectroscopic grade DMSO and DMF as solvents at room temperature. The excitation and emission slit widths were 5 nm. All fluorescence emission spectra are blank-corrected and corrected for instrument-specific effects. The polymer films were prepared by solvent evaporation of polymer solution on the glass substrate. The relative QYs of the polymers were measured using quinine sulfate as the standard. Φ_{FL} of polymer films were measured by Horiba scientific Fluoromax-4 spectrofluorometer with an integral sphere.

3. Results and Discussion

3.1. NMR Analysis

The ^{1}H-NMR spectra of HP–COOH and HP–NH_2 in DMSO-d_6 are shown in Figure 1. For HP–COOH and HP–NH_2, the 1,3,5-trisubstitutedphenyl benzene (1,3,5-TPB) moiety acts as the branching point. All of the possible molecule structures of the obtained polymers (HP–COOH and HP–NH_2) are shown in Scheme 1 with a focus on the functional groups bonded to the 1,3,5-TPB moiety. The number of remaining carboxylic groups (2, 1, or 0) or amino groups (1 or 0) of the 1,3,5-TPB moiety determines the assignment of the terminal unit (T_1 or T_2), linear unit (L_1 or L_2), and dendritic unit (D) [49] as shown in Scheme 1. When the number of remaining carboxylic groups or amino groups is two, the 1,3,5-TPB moiety belongs to T_1 or T_2. When the number of remaining carboxylic groups is one, the 1,3,5-TPB moiety is L_1. When there are no carboxylic groups or amino groups on the 1,3,5-TPB

moiety, it belongs to D. The peaks at about δ = 2.47, and 3.45 ppm are assigned to the protons of DMSO-d_6 and to the absorbed water in the polymers, respectively. For HP–COOH, the peaks near δ = 7.25 and 7.42 ppm are assigned to the protons of the DABBT moieties in the T_1 and T_2 units (see Scheme 1), respectively. The peaks around δ = 7.57 ppm correspond to the protons of the DABBT moiety in the L and D units (see Scheme 1). The peaks near δ = 7.91, 8.00, 8.03, and 8.05 ppm are assigned to the protons of the 1,3,5-TPB moieties in the D units. The peaks around δ = 8.11 and 8.28 ppm correspond to the protons of the 1,3,5-TPB moieties in the L and T_1 units, respectively. The broad peak from δ = 11.0 to 13.0 ppm is assigned to the –COOH end groups of the hyperbranched polyamide. For HP–NH_2, the peaks near δ = 7.12 ppm are assigned to the protons of the DABBT moieties in the T_1 units. The peaks near δ = 7.23, 7.25, and 7.28 ppm are assigned to the protons of the DABBT moieties in the T_2 units. The peaks around δ = 7.40, 7.42, and 7.44 ppm correspond to the protons of the DABBT moiety in the L and D units. The peaks near δ = 7.83, 8.03, and 8.05 ppm are assigned to the protons of the 1,3,5-TPB moieties in the D units. The peaks around δ = 8.11 and 8.27 ppm correspond to the protons of the BTB moieties in the L and T_1 units, respectively. The weak and broad peak from around δ = 11.0 to 13.0 ppm is assigned to the –COOH end groups in the polymer structure, which is much lower than that of HP–COOH.

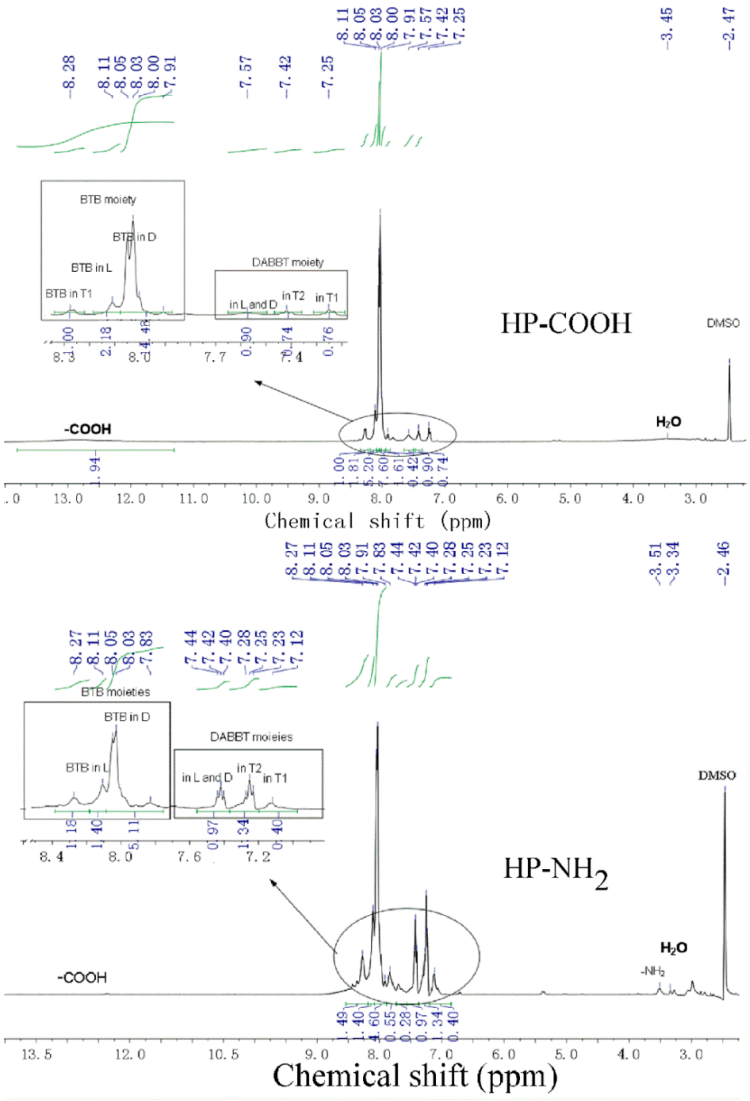

Figure 1. ^{1}H-NMR spectra of HP–COOH and HP–NH_2.

The degree of branching (DB) is one of the most critical structural characteristics for hyperbranched polymers, which describes the structural perfection of hyperbranched polymers. DB was usually defined by Fréchet and coworkers as the following equation: [50]

$$DB = \frac{D + T}{D + T + L} \quad (1)$$

where D, T, and L refer to the number of dendritic, terminal, and linear units in the polymer, respectively. Generally, the values of D, T, and L can be determined by ^{1}H-NMR measurement according to the integrated area of corresponding proton resonance peak. However, unfortunately, in this study, the relative amounts of D, T, and L were difficult to determine by ^{1}H-NMR. As a result, it was hard to calculate the degree of branching (DB).

3.2. FTIR Analysis

The FTIR spectra of HP–COOH and HP–NH_2 are shown in the Supplementary Materials (Figure S5). The absorptions at 1683, 1545, and 1282 cm^{-1} are attributed to the amide groups that derive from the reactions between the –COOH groups of H_3BTB and the –NH_2 groups of DABBT. Concretely, the signal at 1683 cm^{-1} is assigned to the stretching vibration of –C=O, the absorption at 1545 cm^{-1} is assigned to the bending vibration of –N–H, and the absorption at 1282 cm^{-1} is attributed to the stretching vibration of –C–N. The absorptions at 1608 and 1485 cm^{-1} are assigned to the stretching vibration of –C=C– of the aromatic ring. The absorption bands around 1720 and 1233 cm^{-1} are assigned to the stretching vibrations of –C=O and –C–O in –COOH groups [51] and indicate the presence of –COOH groups remaining in both HP–COOH and HP–NH_2. The FTIR analysis and NMR analysis demonstrate that the hyperbranched polybenzobisthiazole amides were successfully synthesized.

3.3. GPC Analysis

The molecular weights and polydispersity index (PDI) values of the hyperbranched polybenzobisthiazole amides were measured using GPC with linear polystyrene as the standard, and the results are shown in Figure 2 and Table 1. The number-average molecular weight (M_n), weight-average molecular weight (M_w), molar mass at the peak maximum (M_p), and the PDI value of HP–COOH are 7426 g/mol, 10,195 g/mol, 12,314 g/mol, and 1.37, respectively. For HP–NH_2, the M_n, M_w, M_p, and the PDI value are 10,280 g/mol, 19,291 g/mol, 11,035 g/mol, and 1.88, respectively (see Table 1). The PDI value of HP–COOH is relatively narrow which is uncommon for a hyperbranched polymer prepared via an $A_2 + B_3$ approach.

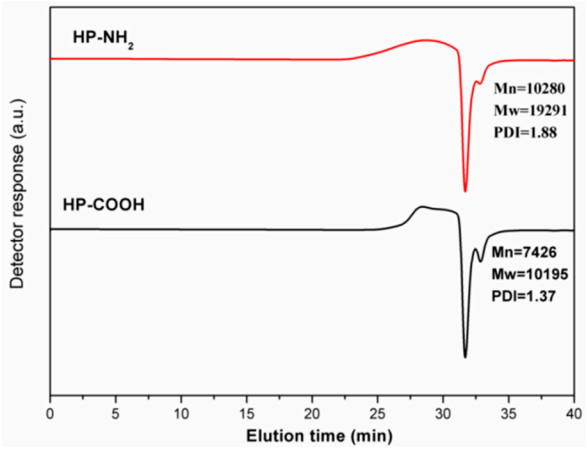

Figure 2. GPC curves of HP–COOH and HP–NH_2.

Table 1. GPC data of HP–COOH and HP–NH_2.

Samples	Monomer Feed Ratio of A_2 to B_3	M_n	M_w	M_p	M_z	M_{z+1}	PDI [a]
HP–COOH	1:1	7426	10,195	12,314	13,387	16,547	1.37
HP–NH_2	9:4	10,280	19,291	11,035	33,938	49,610	1.88

[a] PDI represents polydispersity.

3.4. UV–Vis Absorption and Fluorescence Properties of HP–COOH and HP–NH_2

Figure 3a,b shows the UV–Vis spectra of HP–COOH and HP–NH_2 in the DMSO and DMF solutions, respectively. In Figure 3a, these two polymers display similar absorption behavior in the DMSO and DMF solutions. In the DMSO solution, HP–COOH has a maximum absorption peak at about 285 nm and a shoulder peak at around 336 nm. HP–NH_2 shows a maximum absorption peak at about 283 nm and a shoulder peak at around 336 nm. In the DMF solution (Figure 3b), the maximum absorption peaks of HP–COOH and HP–NH_2 are both at 280 nm. The shoulder peaks of HP–COOH and HP–NH_2 are at around 334 and 342 nm, respectively. The absorptions in the short wavelength region (280–285 nm) are ascribed to π–π^* (π^* means the antibonding orbital) transition and the absorptions in the long wavelength region (333–342 nm) might be due to the intramolecular charge transfer.

The fluorescence spectra of HP–COOH and HP–NH_2 in the DMSO and DMF solutions are shown in Figure 4. The insets in Figure 4 are the intramolecular rotation sketch maps of the two polymers and the photographs of the polymer solutions under both natural light and 365 nm. In the DMF solution, the maximum emission wavelengths (λ_{em}) of HP–COOH and HP–NH_2 are about 518 nm (green light, Figure 4a) and 537 nm (green light, Figure 4b), respectively. The Stokes shifts of HP–COOH and HP–NH_2 in DMF solution are 128 nm (0.79 eV) and 147 nm (0.87 eV), respectively (see Table 2). The corresponding optimal excitation wavelengths (λ_{ex}) of HP–COOH and HP–NH_2 are about 400 and 390 nm, respectively. For HP–COOH in DMF solution, the maximum emission wavelength (λ_{em}) changed from about 518 to 473 nm when the excitation wavelength was varied from 400 to 410 nm. This was the same for HP–NH_2 in the DMF solution (Figure 4b). When the excitation wavelength was changed from 400 to 410 nm, the maximum emission wavelength changed from about 526 to 435 nm. When the excitation wavelength was moved from 410 to 420 nm, the emission intensity of HP–NH_2 decreased rapidly, and the maximum emission wavelength changed from about 435 to 528 nm. Interestingly, there was a saltation in the fluorescence emissions of HP–COOH and HP–NH_2 in the DMF solution when the excitation wavelength was changed from 400 to 410 nm. This may be ascribed to the macromolecular conformational changes [3,52,53] of the polymers that can be converted into one another merely by rotating the single bonds of the molecules when excited by a light with certain energy (as shown in Figure 4a). For the above two polymers, the critical excitation wavelength associated with the chain conformational changes might be 400 nm. In addition, there are moderate emissions in the wavelength range of 400 to 450 nm for both HP–COOH and HP–NH_2 in DMF solutions, which may be ascribed to the intramolecular charge transfer between the donor and acceptor. It is the same for HP–COOH in DMSO solution (Figure 4c). For HP–NH_2 in DMSO (Figure 4d), the emissions belonging to the intramolecular charge transfer are not obvious, which may be merged into the strong and broad emission of HP–NH_2 in DMF.

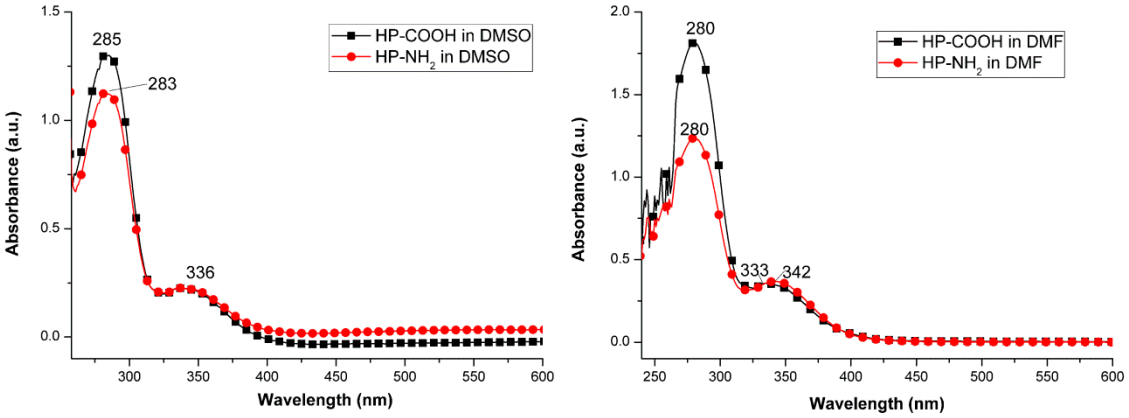

Figure 3. UV–Vis spectra of HP–COOH and HP–NH_2 in: DMSO (**a**); and DMF (**b**) solutions.

Table 2. Photophysical properties of HP–COOH and HP–NH_2.

Samples	λ_{abs} (nm)	λ_{em} (nm)	Stokes Shift (nm/eV) [a]	Eg^{opt} (eV) [b]	Φ_{FL} [c]
HP–COOH in DMSO	285, 336	427, 517	137/0.86	3.13	77.75%
HP–COOH in DMF	280, 333	518	128/0.79	2.55	104.65%
HP–COOH Film	305	436, 462	131/0.42	3.02	2.01%
HP–NH_2 in DMSO	283, 336	529	149/0.92	2.97	81.14%
HP–NH_2 in DMF	280, 342	537	147/0.87	2.76	118.72%
HP–NH_2 Film	301, 339	480	179/0.86	2.55	4.89%

[a] $\triangle E_{Stokes}$ is calculated by the following equation: $\Delta E_{Stokes} = \frac{1240}{\lambda_{ex}} - \frac{1240}{\lambda_{em}}$; [b] optical energy gap (Eg^{opt}) was calculated from the onset of UV–Vis absorption spectra, $Eg^{opt} = 1240/\lambda$; [c] Φ_{FL} represents the fluorescence quantum yields of hyperbranched polymer solutions calculated using quinine sulfate as the standard. The gradient for each sample is proportional to the fluorescence quantum yield of that sample. Conversion into an absolute quantum yield is achieved through the equation given in the text (Equation (1)). Φ_{FL} of polymer films were measured by Horiba scientific Fluoromax-4 spectrofluorometer with an integral sphere.

In the DMSO solution (Figure 4c), HP–COOH had two emission peaks, one is in the relatively short wavelength region (about 428 nm, bluish violet light), and the other in the relatively long wavelength region (around 517 to 542 nm, green light). When the excitation wavelength increased from 340 to 380 nm, the fluorescence intensities at about 542 and 428 nm both increased. Emission in the relatively long wavelength region reached the highest value when excited by light of 380 nm. After that, the emission peak at about 517 nm decreased when the excitation wavelength was further increased to 390 and 400 nm. When excited at 400 nm, the long wavelength region emission disappeared, and the maximum emission changed to the relatively short wavelength region (about 428 nm). This also can be ascribed to the chain conformational changes of the polymers that can be converted into one another merely when excited by light with certain energy. In the DMSO solution, the critical excitation wavelength associated with the chain conformational changes might be 400 nm, which is the same as in the DMF solution. The Stokes shift of HP–COOH in DMSO is 137 nm (0.86 eV), as shown in Table 2.

For HP–NH_2 in the DMSO solution (Figure 4d), when the excitation wavelength changed from 340 to 420 nm, HP–NH_2 displayed a single and broad emission. The maximum emission wavelength (λ_{em}) was at about 529 nm (green light) with an optimal excitation wavelength of 380 nm. The Stokes shift of HP–NH_2 in DMSO (149 nm, 0.92 eV) and in DMF (147 nm, 0.87 eV) are larger than that of HP–COOH in DMSO (137 nm, 0.86 eV) and in DMF (128 nm, 0.79 eV), respectively, as shown in Table 2. For both HP–COOH and HP–NH_2, the Stokes shift in DMSO is larger than that in DMF solutions, which can be ascribed to the polarity of DMSO is higher than that of DMF.

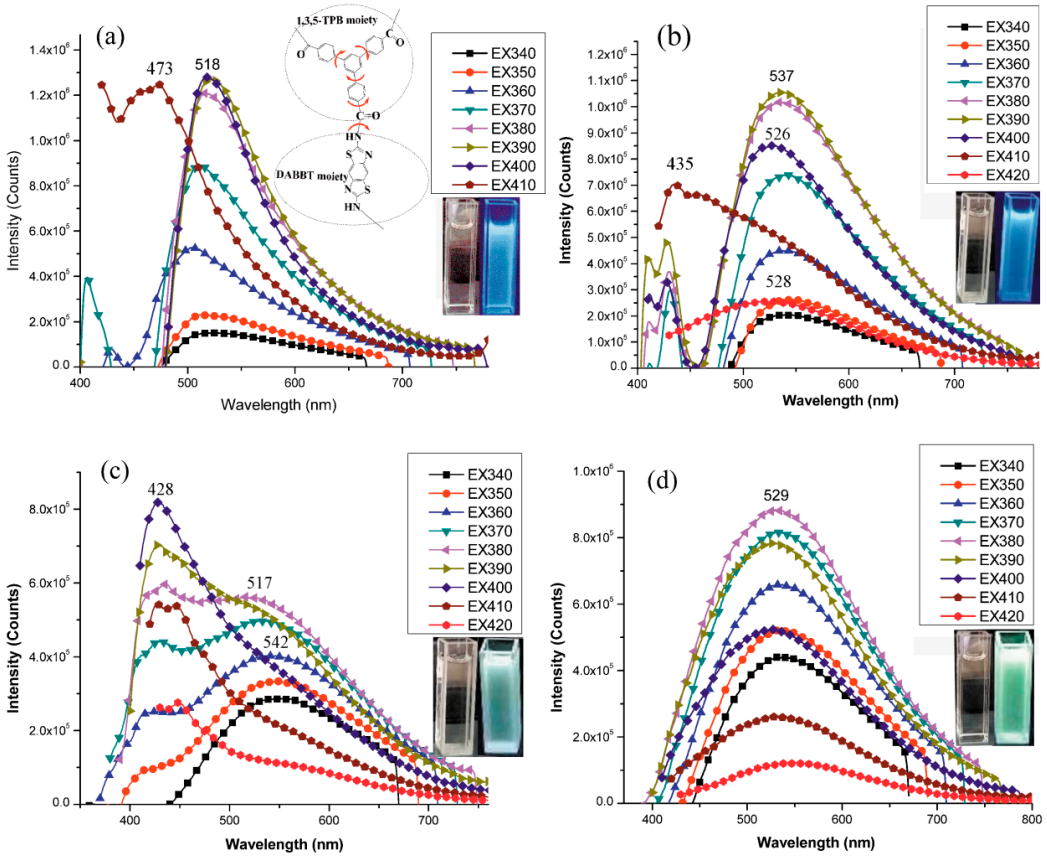

Figure 4. Fluorescence spectra of HP–COOH and HP–NH_2 in DMSO and DMF solutions: (**a**) HP–COOH in DMF (c = 0.135 mg/mL); (**b**) HP–NH_2 in DMF (c = 0.125 mg/mL); (**c**) HP–COOH in DMSO (c = 0.043 mg/mL); and (**d**) HP–NH_2 in DMSO (c = 0.05 mg/mL).

For luminescent materials, QY represents one of the most fundamental and important properties that eventually determines the suitability of materials for applications in optical devices, analysis, bio-sensing, and fluorescence imaging [54,55]. In this work, the fluorescence QYs of the two polymers were obtained relative to quinine sulfate in 0.1 M H_2SO_4 (Φ_{st} = 0.55 [56]), which has a fixed and known fluorescence QY value, according to the following equation:

$$\Phi_x = \Phi_{st}\left(\frac{Grad_x}{Grad_{st}}\right)\left(\frac{\eta_x^2}{\eta_{st}^2}\right) \quad (2)$$

where the subscripts ST and X denote the standard and test sample, respectively; Φ is the fluorescence quantum yield; *Grad* is the gradient from the plot of integrated fluorescence intensity vs. absorbance; and η is the refractive index of the solvent. The fluorescence spectra were measured on a Horiba scientific Fluoromax-4 spectrofluorometer using HPLC grade DMSO and DMF as the solvents at room temperature; excitation and emission slit widths of 5 nm were used. The UV–Vis absorption spectrum and fluorescent spectrum of quinine sulfate in 0.1M H_2SO_4 are shown in the Supplementary Materials (Figures S6 and S7). The fluorescence spectra of both the unknown and the standard samples were obtained under identical conditions. The absorbance and the integrated intensity of the emission spectra were used to calculate the QY. The linear plots for the quinine sulfate standard samples and the two polymers in the DMF or DMSO solutions are shown in Figure 5. The gradient for each sample is proportional to the fluorescence QY of that sample. Conversion to an absolute QY is achieved according to Equation (1). The results are listed in Table 2. The fluorescence QYs of HP–COOH in the DMSO and DMF solutions are 77.75% and 104.65%, respectively, and the fluorescence QYs of HP–NH_2 in

the DMSO and DMF solutions are 81.14% and 118.72%, respectively. The amino-terminated polymer (HP–NH_2) has a relatively higher QY than the carboxyl-terminated polymer (HP–COOH) in the same solvent. This can be attributed to the end group effect of hyperbranched polymers as described in our previous study [39]. The amino group (–NH_2) is an electron donating group and reduces the energy gap between the HOMO and the LUMO, which therefore promotes the corresponding electron transition. There are large numbers of carboxyl groups (–COOH) on the periphery of HP–COOH; –COOH is an electron-withdrawing group and thus weakens fluorescence emission [39]. The two polymers all have relative high QYs in the DMF and DMSO solutions, and in particular, the QYs exceed 100% in the DMF solution. This might be ascribed to the quantum cutting effect where the energy of one absorbed photon is transformed into two or more emitted photons that are usually doped with lanthanide ions [57–59].

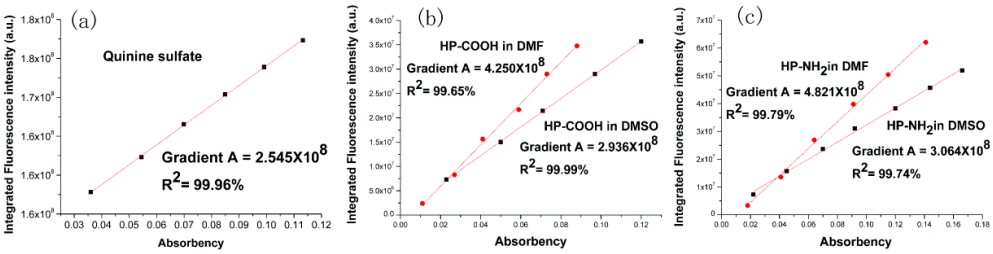

Figure 5. Linear plots for quinine sulfate standard samples and the two polymers: (**a**) quinine sulfate in 0.1 M H_2SO_4; (**b**) HP–COOH in DMF and DMSO; ns (**c**) HP–NH_2 in DMF and DMSO.

According to the above analysis, both HP–COOH and HP–NH_2 have very high fluorescent QY in the DMSO or DMF solutions. Accordingly, the solid films of the two polymers should each have good fluorescent performance. Thus, the HP–COOH and HP–NH_2 films were prepared using a solution evaporation method, and the optical properties of the prepared polymer films were studied. The SEM images of the HP–COOH and HP–NH_2 films are shown in the Supplementary Materials (Figure S8). The UV–Vis spectra of the HP–COOH and HP–NH_2 films are shown in Figure 6. HP–COOH has two absorption peaks at 302 and 308 nm. The maximum absorption is 308 nm. HP–NH_2 shows a maximum absorption at 300 nm and a broad shoulder peak at 341 nm. The maximum absorption wavelength of the HP–COOH film is red-shifted 23 and 28 nm compared to the DMSO and DMF solutions, respectively. The maximum absorption wavelength of the HP–NH_2 film is red-shifted 20 nm compared to the DMSO and DMF solutions. This might be attributed to the increased co-planarity of the hyperbranched polymer molecules in the solid films compared to the solutions. In solution, the two polymers exhibit a more twisted molecular conformation than in the solid film because of rotation about the single bonds of the macromolecules. Thus, the conjugation degree increases, and the maximum UV–Vis absorption is obviously red-shifted in the solid films compared to that in the DMF and DMSO solutions.

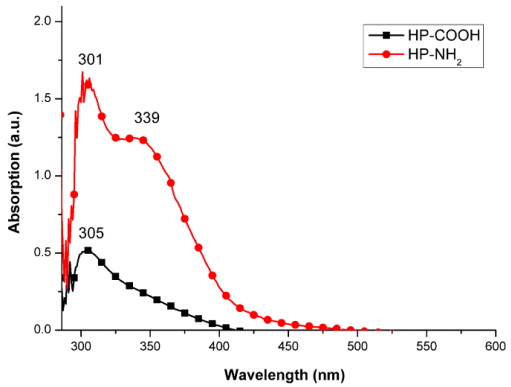

Figure 6. UV–Vis spectra of the HP–COOH and HP–NH_2 films.

Figure 7 shows the fluorescence of the solid films of HP–COOH and HP–NH_2. HP–COOH (Figure 7a) displays two emission peaks at about 436 and 462 nm (blue light) under the excitation wavelength of 340 to 410 nm. The maximum emission wavelength is 436 nm. The optimal excitation wavelength for HP–COOH is 380 nm. The maximum absorption of HP–COOH film is 305 nm, and so the Stokes shift of HP–COOH film is about 131 nm (0.42 eV), as shown in Table 2. When the excitation wavelength was increased from 340 to 380 nm, the emission intensities gradually increased. When the excitation wavelength was increased from 380 to 410 nm, the emission intensities decreased. In particular, when the excitation wavelength was increased from 400 to 410 nm, the fluorescence intensity reduced significantly. HP–NH_2 exhibits a single fluorescence emission centered at about 480 nm (blue light), as shown in Figure 7b. The optimal excitation wavelength for HP–NH_2 is 460 nm. The maximum absorption of HP–NH_2 film is 300 nm, and so the Stokes shift of HP–NH_2 film is about 179 nm (0.86 eV), as shown in Table 2, which is larger than that of HP–COOH film. The fluorescence quantum yields of the two hyperbranched polymers films were measured by Horiba scientific Fluoromax-4 spectrofluorometer with an integral sphere. The excitation wavelengths were 380 and 360 nm for HP–COOH and HP–NH_2, respectively. The fluorescent QYs of HP–COOH and HP–NH_2 films are 2.01% and 4.89%, respectively, which is much lower than that in DMSO or DMF solutions. This might be due to the aggregation-induced quenching effect (ACQ) [60]. The large effective Stokes shifts (0.42 to 0.92 eV) of the two polymers may be useful to minimize the self-absorption and light scattering in optical materials [61,62]. These two polymers are promising candidates for luminescent solar concentrators and blue light emitting materials.

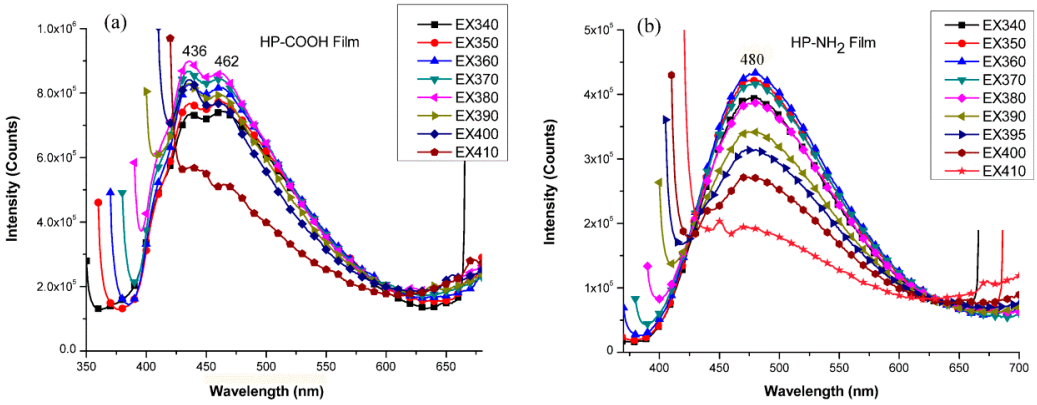

Figure 7. Fluorescence curves of: (**a**) HP–COOH; and (**b**) HP–NH_2 in the solid films.

To understand the electronic structures of the two synthesized polymers, DFT calculations of three selected oligomers were performed by standard computational methods and basis sets using Gaussian 09 software (Gaussian Inc., Wallingford, the United States) package. The HOMO and LUMO wave functions and energy gaps of three selected oligomers are illustrated in Figure 8. Oligomer 1 represents the dendrimer unit (D, Scheme 1) or the terminal unit (T_2, Scheme 1) of the hyperbranched polymers, in which the carboxyl groups of H_3BTB are all reacted with amino groups of DABBT to form amide bond. The molecular weight of Oligomer 1 is 1051 g/mol. Oligomer 2 represents the terminal unit (T_1, Scheme 1) of the hyperbranched polymers, in which the carboxyl groups is excessive and the amino groups are consumed to generate amide. The molecular weight of Oligomer 2 is 1063 g/mol. Oligomer 3 represents the linear unit (L, Scheme 1) of the hyperbranched polymers, in which two carboxyl groups of H_3BTB are consumed and one carboxyl group remain. The molecular weight of Oligomer 3 is 847 g/mol. The HOMO is localized on the Pi orbital (π–orbital) of the DABBT unit for the three oligomers, while the LUMO is strongly localized on the π–orbital of the H_3BTB unit for the three oligomers. The two hyperbranched polymers have twisted structure with DABBT as a donor unit and H_3BTB as an acceptor unit. The HOMO and LUMO were effectively separated. The energy gaps were 3.49 eV (Oligomer 1), 3.87 eV (Oligomer 2), and 3.45 eV (Oligomer 3), respectively. The effective

HOMO–LUMO separation helps to induce the intramolecular charge transfer transition from HOMO to LUMO [63,64]. There observations corroborate well with the UV–Vis absorption and fluorescence properties of HP–COOH and HP–NH_2.

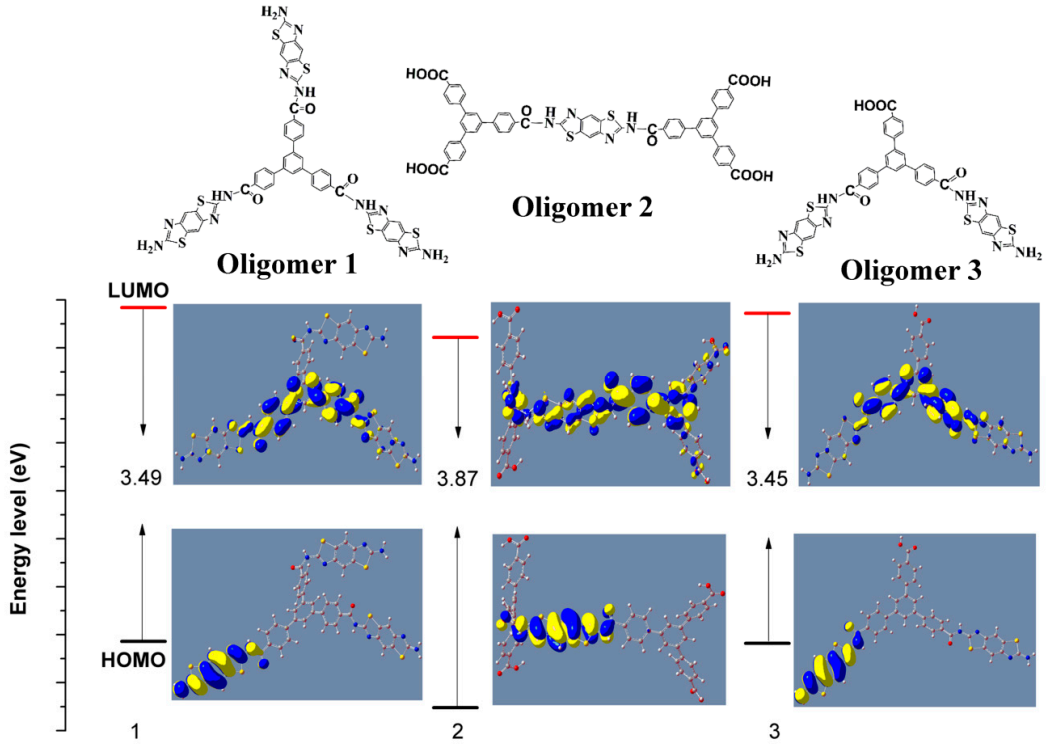

Figure 8. Visualization of HOMO, LUMO and energy gaps of three oligomers calculated by Gaussian 09 software package.

3.5. XRD Analysis

The wide angle X-ray diffraction (WAXD) spectra of HP–COOH and HP–NH_2 are shown in Figure 9. HP–COOH has two weak and broad diffraction peaks at about 2θ = 18.92° and 24.90°, indicating that this polymer is almost amorphous with certain crystallinity. For HP–NH_2, there are an intense and sharp peak at 2θ = 17.45° and three weak peaks at about 2θ = 10.02°, 20.56°, and 25.20°, illustrating that HP–NH_2 is a semi-crystalline polymer.

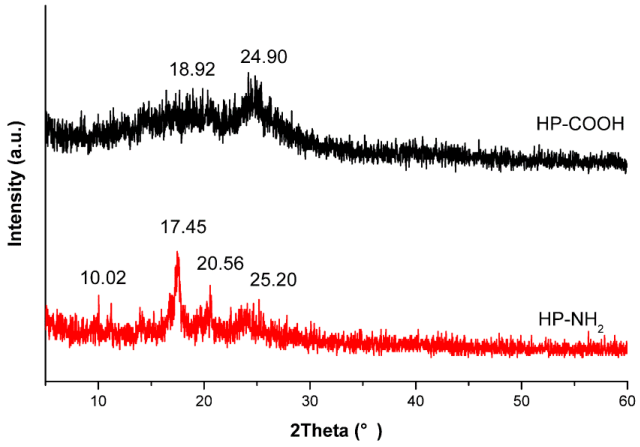

Figure 9. Wide angle X-ray diffraction (WAXD) spectra of HP–COOH and HP–NH_2.

3.6. Thermal Analysis

The TGA and DSC thermograms of HP–COOH and HP–NH_2 are shown in Figure 10. The two polymers display similar thermal degradation behavior in the range of 30 to 800 °C. There are two stages in the TGA curves of HP–COOH and HP–NH_2. The first stage is from 30 °C to about 282 °C, with weight losses of 6.95% and 8.57% for HB–COOH and HB–NH_2, respectively. The weight losses in this stage were ascribed to the slow removal of the absorbed water from the hyperbranched polymers. The second stage is from about 282 °C to about 800 °C. The weight loss in this second stage is much higher than that in the first stage, and this is because of the decomposition of the synthesized polymers. The residual masses at 800 °C are about 60.8% and 61.3% for HB–COOH and HB–NH_2, respectively. The thermal stability of HB–COOH is higher than that of HB–NH_2 in the temperature range of 282 to about 583 °C. From 583 to about 800 °C, the thermal stability of HB–NH_2 is slightly higher than that of HB–COOH.

The DSC curves of HB–COOH and HB–NH_2 display wide endothermic peaks at about 93 and 82.5 °C, respectively, and this is because of the glass transition of the synthesized polymers. The endothermic peaks centered at about 282 and 264 °C might be ascribed to the melting point (T_m) of the crystallization regions of HP–COOH and HP–NH_2, respectively, because both HP–NH_2 and HP–COOH have certain crystallinity as displayed in their XRD curves (Figure 9). The endothermic peaks centered at about 301 and 371 °C might be ascribed to the thermal decomposition temperature (T_d) of HP–COOH and HP–NH_2, respectively. These two polymers have relatively high thermal stability under the temperature of 260 °C.

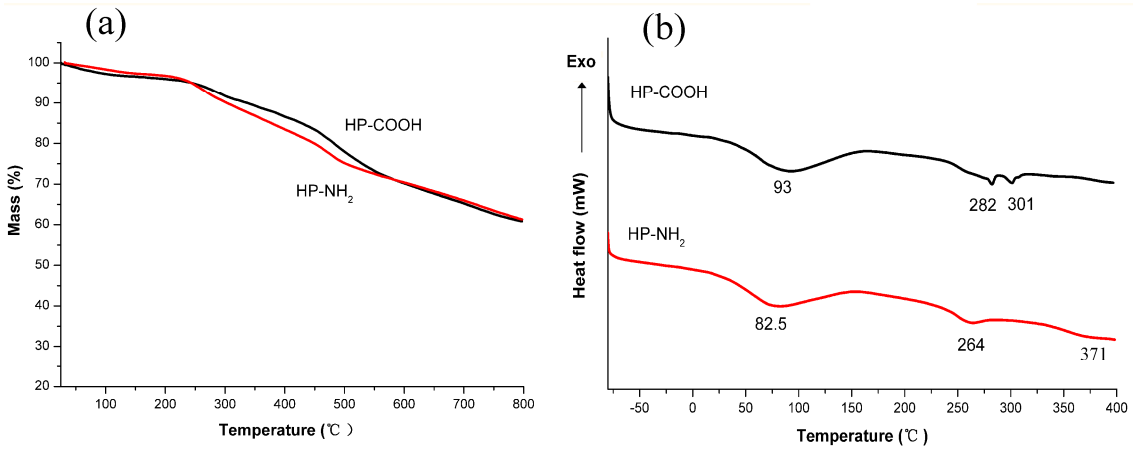

Figure 10. (**a**) TGA; and (**b**) DSC curves of HP–COOH and HP–NH_2.

4. Conclusions

Two novel highly fluorescent hyperbranched polybenzobisthiazole amides with different terminal groups were synthesized via the $A_2 + B_3$ approach using H_3BTB and DABBT as reaction materials, by regulating the mole ratio of the monomers. The prepared polymers were characterized using FTIR and ^{1}H-NMR analysis. GPC analysis showed that the M_n, M_w, and PDI of HP–COOH and HP–NH_2 were 7426 g/mol, 10,195 g/mol, and 1.37, respectively. The M_n, M_w, and PDI of HP–NH_2 were 10,280 g/mol, 19,291 g/mol and 1.88, respectively. The two polymers are soluble in DMSO and DMF. Their solutions mainly emitted strong green light (517–537 nm) when the excitation wavelength varied from 340 to 410 nm. The relative fluorescence QYs in the DMSO solution were calculated as 77.75% and 81.14% with the Stokes shifts of 137 nm (0.86 eV) and 149 nm (0.92 eV) for HP–COOH and HP–NH_2, respectively, using quinine sulfate as the standard. In the DMF solution, the relative fluorescence QYs of HP–COOH and HP–NH_2 were calculated as 104.65% and 118.72%, with the Stokes shifts of 128 nm (0.79 eV) and 147 nm (0.87 eV), respectively. Their films mainly emitted strong blue light with the maximum emission wavelength of 436 nm and 480 nm for HP–COOH and HP–NH_2, respectively. The Stokes

shifts for HP–COOH and HP–NH_2 films were 131 nm (0.42 eV) and 179 nm (0.86 eV), respectively. DFT calculations demonstrated that the HOMO and LUMO were effectively separated with DABBT as a donor unit and H_3BTB as an acceptor unit. The effective HOMO–LUMO separation helps to induce the intramolecular charge transfer transition from HOMO to LUMO. The two hyperbranched polymers possess the merits of large Stokes shift and high fluorescence quantum yield, which may simultaneously solve the problems of nonradioactive re-absorption of many fluorescent materials, and may become promising candidates as luminescent solar concentrators for photovoltaic devices and blue light emitting materials.

Supplementary Materials: The following are available online at www.mdpi.com/2073-4360/9/8/304/s1, Figure S1: ^{1}H–NMR spectrum of DABBT, Figure S2: ^{13}C–NMR spectrum of DABBT, Figure S3: ^{1}H–NMR spectrum of H_3BTB, Figure S4: ^{13}C–NMR spectrum of H_3BTB, Figure S5: FTIR spectra of HP–COOH and HP–NH_2, Figure S6: the UV–Vis absorption spectrum of quinine sulfate in 0.1 M H_2SO_4, Figure S7: the fluorescent spectrum of quinine sulfate in 0.1 M H_2SO_4, Figure S8: SEM images of: HP–COOH film (A,B); and HP–NH_2 film (C,D).

Acknowledgments: The author thanks the scientific research project fund of Shaanxi Province Key Laboratory of Phytochemistry of China (14JS006) and the Doctoral research start-up project fund of Baoji University of Arts and Sciences (ZK2017032) for the support. The author thanks Dongmei Wang for her assistance with theoretical arithmetic.

Conflicts of Interest: The author declares no conflict of interest.

References

1. Huang, W.; Smarsly, E.; Han, J.S.; Bender, M.; Seehafer, K.; Wacker, I.; Schröder, R.R.; Bunz, U.H.F. Truxene-Based Hyperbranched Conjugated Polymers: Fluorescent Micelles Detect Explosives in Water. *ACS Appl. Mater. Interfaces* **2017**, *9*, 3068–3074. [CrossRef] [PubMed]
2. Li, H.B.; Wu, X.F.; Xu, Y.X.; Tong, H.; Wang, L.X. Dicyanovinyl-functionalized fluorescent hyperbranched conjugated polymer nanoparticles for sensitive naked-eye cyanide ion detection. *Polym. Chem.* **2014**, *5*, 5949–5956. [CrossRef]
3. Liu, J.Z.; Zhong, Y.C.; Lu, P.; Hong, Y.N.; Lam, J.W.Y.; Faisal, M.; Yu, Y.; Wong, K.S.; Tang, B.Z. A superamplification effect in the detection of explosives by a fluorescent hyperbranched poly(silylenephenylene) with aggregation-enhanced emission characteristics. *Polym. Chem.* **2010**, *1*, 426–429. [CrossRef]
4. Chen, L.; Gao, Y.X.; Fu, Y.Y.; Zhu, D.F.; He, Q.G.; Cao, H.M.; Cheng, J.G. Borate ester endcapped fluorescent hyperbranched conjugated polymer for trace peroxide explosive vapor detection. *RSC Adv.* **2015**, *5*, 29624–29630. [CrossRef]
5. Jiang, H.B.; Wu, P.C.; Zhang, Y.; Jiao, Z.N.; Xu, W.; Zhang, X.T.; Fu, Y.Y.; He, Q.G.; Cao, H.M.; Cheng, J.G. Hyperbranched polymer based fluorescent probes for ppt level nerve agent simulant vapor detection. *Anal. Methods* **2017**, *9*, 1748–1754. [CrossRef]
6. Armelin, E.; Whelan, R.; Martínez-Triana, Y.M.; Aleman, C.; Finn, M.G.; Díaz, D.D. Protective Coatings for Aluminum Alloy Based on Hyperbranched 1,4-Polytriazoles. *ACS Appl. Mater. Interfaces* **2017**, *9*, 4231–4243. [CrossRef] [PubMed]
7. Zigmond, J.S.; Pavía-Sanders, A.; Russell, J.D.; Wooley, K.L. Dynamic Anti-Icing Coatings: Complex, Amphiphilic Hyperbranched Fluoropolymer Poly(ethylene glycol) Cross-Linked Networks with an Integrated Liquid Crystalline Comonomer. *Chem. Mater.* **2016**, *28*, 5471–5479. [CrossRef]
8. Li, Y.; Wang, L.; Li, B.; Zhang, M.C.; Wen, R.; Guo, X.H.; Li, X.; Zhang, J.; Li, S.J.; Ma, L.J. Pore-Free Matrix with Cooperative Chelating of Hyperbranched Ligands for High-Performance Separation of Uranium. *ACS Appl. Mater. Interfaces* **2016**, *8*, 28853–28861. [CrossRef] [PubMed]
9. Duan, S.; Yu, B.G.; Gao, C.X.; Yuan, W.; Ma, J.; Xu, F.-J. A Facile Strategy to Prepare Hyperbranched Hydroxyl-Rich Polycations for Effective Gene Therapy. *ACS Appl. Mater. Interfaces* **2016**, *8*, 29334–29342. [CrossRef] [PubMed]
10. Wang, S.Q.; Chen, R.J. pH-Responsive, Lysine-Based, Hyperbranched Polymers Mimicking Endosomolytic Cell-Penetrating Peptides for Efficient Intracellular Delivery. *Chem. Mater.* **2017**. [CrossRef]
11. Ma, N.; Zhao, L.R.; Hu, X.Y.; Yin, Z.; Zhang, Y.F.; Meng, J.Q. Protein Transport Properties of PAN Membranes Grafted with Hyperbranched Polyelectrolytes and Hyperbranched Zwitterions. *Ind. Eng. Chem. Res.* **2017**, *56*, 1019–1028. [CrossRef]

12. Liu, G.H.; Zhang, G.F.; Hu, J.M.; Wang, X.R.; Zhu, M.Q.; Liu, S.Y. Hyperbranched Self-Immolative Polymers (hSIPs) for Programmed Payload Delivery and Ultrasensitive Detection. *J. Am. Chem. Soc.* **2015**, *137*, 11645–11655. [CrossRef] [PubMed]
13. Huang, X.; Ishitobi, H.; Inouye, Y. Formation of fluorescent platinum nanoclusters using hyper-branched polyethylenimine and their conjugation to antibodies for bio-imaging. *RSC Adv.* **2016**, *6*, 9709–9716. [CrossRef]
14. Sun, P.; Chen, D.; Deng, H.P.; Wang, N.; Huang, P.; Jin, X.; Zhu, X.Y. "Bottom-up" Construction of Multi-Polyprodrug-Arm Hyperbranched Amphiphiles for Cancer Therapy. *Bioconj. Chem.* **2017**, *28*, 1470–1480. [CrossRef] [PubMed]
15. Tian, K.; Jia, X.; Zhao, X.; Liu, P. Biocompatible Reduction and pH Dual-Responsive Core Cross-Linked Micelles Based on Multifunctional Amphiphilic Linear–Hyperbranched Copolymer for Controlled Anticancer Drug Delivery. *Mol. Pharm.* **2017**, *14*, 799–807. [CrossRef] [PubMed]
16. Heckert, B.; Banerjee, T.; Sulthana, S.; Naz, S.; Alnasser, R.; Thompson, D.; Normand, G.; Grimm, J.; Perez, J.M.; Santra, S. Design and Synthesis of New Sulfur-Containing Hyperbranched Polymer and Theranostic Nanomaterials for Bimodal Imaging and Treatment of Cancer. *ACS Macro Lett.* **2017**, *6*, 235–240. [CrossRef]
17. Wu, Y.G.; Hao, X.H.; Wu, J.L.; Jin, J.; Ba, X.W. Pure Blue-Light-Emitting Materials: Hyperbranched Ladder-Type Poly(*p*-phenylene)s Containing Truxene Units. *Macromolecules* **2010**, *43*, 731–738. [CrossRef]
18. Li, Z.A.; Ye, S.H.; Liu, Y.Q.; Yu, G.; Wu, W.B.; Qin, J.G.; Li, Z. New Hyperbranched Conjugated Polymers Containing Hexaphenylbenzene and Oxadiazole Units: Convenient Synthesis and Efficient Deep Blue Emitters for PLEDs Application. *J. Phys. Chem. B* **2010**, *114*, 9101–9108. [CrossRef] [PubMed]
19. Qin, A.J.; Lam, J.W.Y.; Jim, C.K.W.; Zhang, L.; Yan, J.J.; Häussler, M.; Liu, J.Z.; Dong, Y.Q.; Liang, D.H.; Chen, E.Q.; et al. Hyperbranched Polytriazoles: Click Polymerization, Regioisomeric Structure, Light Emission, and Fluorescent Patterning. *Macromolecules* **2008**, *41*, 3808–3822. [CrossRef]
20. Wen, X.; Zhang, D.X.; Ren, T.C.; Xiao, J.C.; Wu, Y.G.; Bai, L.B.; Ba, X.W. Yellow emitting materials: Truxene-based conjugated hyperbranched polymer containing difluoroboron-diketonate complexes. *Dyes Pigments* **2017**, *137*, 437–444. [CrossRef]
21. Sun, J.; Yang, J.L.; Zhang, C.Y.; Wang, H.; Li, J.; Su, S.J.; Xu, H.X.; Zhang, T.M.; Wu, Y.L.; Wong, W.-Y.; et al. A novel white-light-emitting conjugated polymer derived from polyfluorene with a hyperbranched structure. *New J. Chem.* **2015**, *39*, 5180–5188. [CrossRef]
22. Wu, Y.L.; Li, J.; Liang, W.Q.; Yang, J.L.; Sun, J.; Wang, H.; Liu, X.G.; Xu, B.S.; Huang, W. Hyperbranched fluorene-alt-carbazole copolymers with spiro[3.3]heptane-2,6-dispirofluorene as the core and their application in white polymer light-emitting devices. *RSC Adv.* **2015**, *5*, 49662–49670. [CrossRef]
23. Kim, J.; Park, J.; Jin, S.-H.; Lee, T.S. Synthesis of conjugated, hyperbranched copolymers for tunable multicolor emissions in light-emitting diodes. *Polym. Chem.* **2015**, *6*, 5062–5069. [CrossRef]
24. Xing, L.-B.; Wang, X.-J.; Zhang, J.-L.; Zhou, Z.Y.; Zhuo, S.P. Tetraphenylethene-containing supramolecular hyperbranched polymers: Aggregation-induced emission by supramolecular polymerization in aqueous solution. *Polym. Chem.* **2016**, *7*, 515–518. [CrossRef]
25. Du, Y.Q.; Yan, H.X.; Niu, S.; Bai, L.H.; Chai, F. Facile one-pot synthesis of novel water-soluble fluorescent hyperbranched poly(amino esters). *RSC Adv.* **2016**, *6*, 88030–88037. [CrossRef]
26. Fu, X.; Zhang, Q.W.; Wu, G.; Zhou, W.; Wang, Q.-C.; Qu, D.-H. BODIPY-based conjugated microporous polymers as reusable heterogeneous photosensitisers in a photochemical flow reactor. *Polym. Chem.* **2014**, *5*, 6662–6670. [CrossRef]
27. Scott, M.G.; Fréchet, J.M.J. Convergent Dendrons and Dendrimers: From Synthesis to Applications. *Chem. Rev.* **2001**, *101*, 3819–3868. [CrossRef]
28. Matthew, R.R.; Wang, S.; Guillermo, C.B.; Cao, Y. Electroluminescence from Well-Defined Tetrahedral Oligophenylenevinylene Tetramers. *Adv. Mater.* **2000**, *12*, 1701–1704. [CrossRef]
29. Chen, H.; Kong, J. Hyperbranched polymers from A_2 + B_3 strategy: Recent advances in description and control of fine topology. *Polym. Chem.* **2016**, *7*, 3643–3663. [CrossRef]
30. Wu, W.B.; Ye, C.; Qin, J.G.; Li, Z. The Utilization of Isolation Chromophore in an "A_3+B_2" Type Second-Order Nonlinear Optical Hyperbranched Polymer. *Macromol. Rapid Commun.* **2013**, *34*, 1072–1079. [CrossRef] [PubMed]

31. Jikei, M.; Chon, S.-H.; Kakimoto, M.; Kawauchi, S.; Imase, T.; Watanebe, J. Synthesis of Hyperbranched Aromatic Polyamide from Aromatic Diamines and Trimesic Acid. *Macromolecules* **1999**, *32*, 2061–2064. [CrossRef]
32. Young, H.K. Hyperbranched polymers 10 years after. *J. Polym. Sci. Part A Polym. Chem.* **1998**, *36*, 1685–1698. [CrossRef]
33. Kudo, H.; Matsubara, S.; Yamamoto, H.; Kozawa, T. Synthesis of hyperbranched polyacetals via $a_n + b_2$-type polyaddition (n = 3, 8, 18, and 21): Candidate resists for extreme ultraviolet lithography. *J. Polym. Sci. Part A Polym. Chem.* **2015**, *53*, 2343–2350. [CrossRef]
34. Herrema, J.K.; Wildeman, J.; Gil, R.E.; van Hutten, P.F.; Wieringa, R.H.; Hadziioannou, G. Tuning of the Luminescence in Multiblock Alternating Copolymers. 1. Synthesis and Spectroscopy of Poly [(silanylene)thiophene]s. *Macromolecules* **1995**, *28*, 8102–8116. [CrossRef]
35. Lee, J.W.; Wang, C.S. Processing of optical quality rigid-rod polymer thin films. *Polymer* **1994**, *35*, 3673–3678. [CrossRef]
36. Roberts, M.F.; Jenekhe, S.A.; Cameron, A.; Mcmillan, M.; Perlstein, J. Lewis Acid Coordination Complexes of Polymers. 2. Computational Modeling of Single-Chain and Aggregate Structures of Rigid-Rod Poly (*p*-phenylenebenzobisthiazole). *Chem. Mater.* **1994**, *6*, 658–670. [CrossRef]
37. Bai, S.J.; Spry, R.J.; Zelmon, D.E.; Ramabadran, U.; Jackson, J. Optical anisotropy of polymeric films measured by waveguide propagation mode determination. *J. Polym. Sci. Part B Polym. Phys.* **1992**, *30*, 1507–1514. [CrossRef]
38. Vanherzeele, H.; Meth, J.S.; Jenekhe, S.A.; Roberts, M.F. Third-order nonlinear optical properties of thin films of poly(*p*-phenylene benzobisthiazole) and its molecular composites with polyamides. *Appl. Phys. Lett.* **1991**, *58*, 663–665. [CrossRef]
39. Hu, X.B.; Yu, D.M. Hyperbranched Polybenzobisthiazole with High Thermal Stability, Good Organosolubility, and Interesting Optical Performance. *Macromol. Chem. Phys.* **2012**, *213*, 738–746. [CrossRef]
40. Hu, X.B. Synthesis and properties of novel benzobisthiazole-containing hyperbranched polyamides derived from 2,6-diaminobenzo[1,2-d:4,5-d']bisthiazole. *J. Appl. Polym. Sci.* **2016**, *133*. [CrossRef]
41. Li, J.; Bo, Z.S. "AB_2 + AB" Approach to Hyperbranched Polymers Used as Polymer Blue Light Emitting Materials. *Macromolecules* **2004**, *37*, 2013–2015. [CrossRef]
42. Dutta, T.; Woody, K.B.; Parkin, S.R.; Watson, M.D.; Gierschner, J. Conjugated Polymers with Large Effective Stokes Shift: Benzobisdioxole-Based Poly(phenylene ethynylene)s. *J. Am. Chem. Soc.* **2009**, *131*, 17321–17327. [CrossRef] [PubMed]
43. Kumar, G.R.; Sarkar, S.K.; Thilagar, P. Aggregation-Induced Emission and Sensing Characteristics of Triarylborane–Oligothiophene–Dicyanovinyl Triads. *Chem. Eur. J.* **2016**, *22*, 17215–17225. [CrossRef] [PubMed]
44. Zhang, Q.S.; Kuwabara, H.; Potscavage, W.J.; Huang, S.P.; Hatae, Y.; Shibata, T.; Adachi, C. Anthraquinone-Based Intramolecular Charge-Transfer Compounds: Computational Molecular Design, Thermally Activated Delayed Fluorescence, and Highly Efficient Red Electroluminescence. *J. Am. Chem. Soc.* **2014**, *136*, 18070–18081. [CrossRef] [PubMed]
45. Gan, S.F.; Luo, W.W.; He, B.R.; Chen, L.; Nie, H.; Hu, R.G.; Qin, A.J.; Zhao, Z.J.; Tang, B.Z. Integration of aggregation-induced emission and delayed fluorescence into electronic donor–acceptor conjugates. *J. Mater. Chem. C* **2016**, *4*, 3705–3708. [CrossRef]
46. Hu, X.B. Novel fluorescent porous hyperbranched aromatic polyamide containing 1,3,5-triphenylbenzene moieties: Synthesis and characterization. *J. Appl. Polym. Sci.* **2017**, *134*. [CrossRef]
47. Wolfe, F.; Loo, B.H.; Arnold, F.E. Rigid-rod polymers. 2. Synthesis and thermal properties of para-aromatic polymers with 2,6-benzobisthiazole units in the main chain. *Macromolecules* **1981**, *14*, 915–920. [CrossRef]
48. Osaheni, J.A.; Jenekhe, S.A. Synthesis and processing of heterocyclic polymers as electronic, optoelectronic, and nonlinear optical materials. 1. New conjugated rigid-rod benzobisthiazole polymers. *Chem. Mater.* **1992**, *4*, 1282–1290. [CrossRef]
49. Komber, H.; Voit, B.; Monticelli, O.; Russo, S. ^{1}H and ^{13}C-NMR Spectra of a Hyperbranched Aromatic Polyamide from *p*-Phenylenediamine and Trimesic Acid. *Macromolecules* **2001**, *34*, 5487–5493. [CrossRef]
50. Hawker, C.J.; Lee, R.; Fréchet, J.M.J. One-step synthesis of hyperbranched dendritic polyesters. *J. Am. Chem. Soc.* **1991**, *113*, 4583–4588. [CrossRef]
51. Xu, H.J.; Chen, K.C.; Guo, X.X.; Fang, J.H.; Yin, J. Synthesis and properties of hyperbranched polybenzimidazoles via $A_2 + B_3$ approach. *J. Polym. Sci. Part A Polym. Chem.* **2007**, *45*, 1150–1158. [CrossRef]

52. Chen, B.; Zhang, H.; Luo, W.; Nie, H.; Hu, R.; Qin, A.; Zhao, Z.; Tang, B.Z. Oxidation-enhanced emission: Exploring novel AIEgens from thieno[3,2-b]thiophene S,S-dioxide. *J. Mater. Chem. C* **2017**, *5*, 960–968. [CrossRef]
53. Gao, M.; Su, H.; Lin, Y.; Ling, X.; Li, S.; Qin, A.; Tang, B.Z. Photoactivatable aggregation-induced emission probes for lipid droplets-specific live cell imaging. *Chem. Sci.* **2017**, *8*, 1763–1768. [CrossRef]
54. Chen, B.; Nie, H.; Hu, R.; Qin, A.; Zhao, Z.; Tang, B.Z. Insights into the correlation between the molecular conformational change and AIE activity of 2,5-bis(dimesitylboryl)-3,4-diphenylsiloles. *J. Mater. Chem. C* **2016**, *4*, 7541–7545. [CrossRef]
55. Hu, J.; Zhang, C.-Y. Simple and Accurate Quantification of Quantum Yield at the Single-Molecule/Particle Level. *Anal. Chem.* **2013**, *85*, 2000–2004. [CrossRef] [PubMed]
56. Melhuish, W.H. Quantum efficiencies of fluorescence of organic substances: Effect of solvent and concentration of the fluorescent solute. *J. Phys. Chem.* **1961**, *65*, 229–235. [CrossRef]
57. Dexter, D.L. Possibility of Luminescent Quantum Yields Greater than Unity. *Phys. Rev.* **1957**, *108*, 630–633. [CrossRef]
58. Lorbeer, C.; Cybinska, J.; Mudring, A.V. Reaching quantum yields ≫100% in nanomaterials. *J. Mater. Chem. C* **2014**, *2*, 1862–1868. [CrossRef]
59. Wegh, R.T.; Donker, H.; Oskam, K.D.; Meijerink, A. Visible Quantum Cutting in $LiGdF_4$:Eu^{3+} Through Downconversion. *Science* **1999**, *283*, 663–666. [CrossRef] [PubMed]
60. Sasanka, D.; Enquan, J.; Matthew, A.; Thomas, H.; Donglin, J. Highly Emissive Covalent Organic Frameworks. *J. Am. Chem. Soc.* **2016**, *138*, 5797–5800. [CrossRef]
61. Banal, J.L.; Zhang, B.L.; Jones, D.J.; Ghiggino, K.P.; Wong, W.W.H. Emissive Molecular Aggregates and Energy Migration in Luminescent Solar Concentrators. *Acc. Chem. Res.* **2017**, *50*, 49–57. [CrossRef] [PubMed]
62. Mukherjee, K.; Chio, T.I.; Gu, H.; Banerjee, A.; Sorrentino, A.M.; Sackett, D.L.; Bane, S.L. Benzocoumarin Hydrazine: A Large Stokes Shift Fluorogenic Sensor for Detecting Carbonyls in Isolated Biomolecules and in Live Cells. *ACS Sens.* **2017**, *2*, 128–134. [CrossRef] [PubMed]
63. Tanaka, H.; Shizu, K.; Nakanotani, H.; Adachi, C. Twisted Intramolecular Charge Transfer State for Long-Wavelength Thermally Activated Delayed Fluorescence. *Chem. Mater.* **2013**, *25*, 3766–3771. [CrossRef]
64. Kim, B.-G.; Ma, X.; Chen, C.; Le, Y.; Coir, E.W.; Hashemi, H.; Aso, Y.; Green, P.F.; Kieffer, J.; Kim, J. Energy Level Modulation of HOMO, LUMO, and Band-Gap in Conjugated Polymers for Organic Photovoltaic Applications. *Adv. Funct. Mater.* **2013**, *23*, 439–445. [CrossRef]